The yield and isotopic composition of radiolytic H_2, a potential energy source for the deep subsurface biosphere

Li-Hung Lin[1*], Greg F. Slater[2,3], Barbara Sherwood Lollar[2], Georges Lacrampe-Couloume[2], and T. C. Onstott[1]

[1]Department of Geosciences, Princeton University, Princeton, NJ, USA

[2]Stable Isotope Laboratory, Department of Geology, University of Toronto, Toronto, ON, Canada

[3]Woods Hole Oceanographic Institute, MA, USA

*Corresponding author at present address: Geophysical Laboratory, 5251 Broad Branch Rd., N.W., Washington, DC 20015, USA; email: l.lin@gl.ciw.edu.

Abstract

The production rate and isotopic composition of H_2 derived from radiolytic reactions in H_2O were measured to assess the importance of radiolytic H_2 in subsurface environments and to determine whether its isotopic signature can be used as a diagnostic tool. Saline and pure, aerobic and anaerobic water samples with pH values of 4, 7 and 10 were irradiated in sealed vials at room temperature with an artificial γ source, and the H_2 abundance in the headspace and its isotopic composition were measured. The H_2 concentrations were observed to increase linearly with dosage at a rate of 0.40 ± 0.04 molecules $(100\ eV)^{-1}$ within the dosage range of 900 to 3500 Gray (Gy; Gy =1 J Kg^{-1}) with no indication of a maximum limit on H_2 concentration. At ~2000 Gy, the H_2 concentration varied only by 16% across the experimental range of pH, salinity and O_2. Based upon this measured yield and H_2 yields for α and β particles a radiolytic H_2 production rate of 10^{-9} to 10^{-4} nM sec^{-1} was estimated for the range of radioactive element concentrations and porosities typical of crustal rocks. The δD of H_2 ($\delta D = ((D/H)_{sample}/(D/H)_{standard} - 1) \times 1000$) was independent of the dosage, pH (except for pH 4), salinity, and O_2 and yielded an $\alpha D_{H2O\text{-}H2}$ of 2.05 ± 0.07 ($\alpha D_{H2O\text{-}H2} = (D/H)_{H2O}$ to $(D/H)_{H2}$), slightly less than predicted radiolytic models. Although this radiolytic fractionation value is significantly heavier than that of equilibrium isotopic exchange between H_2 and H_2O, the isotopic exchange rate between H_2 and H_2O will erase the heavy δD of radiolytic H_2 if the age of the groundwater is greater than ~10^3 to 10^4 years. The millimolar concentrations of H_2 observed in the groundwater of several Precambrian Shields are consistent with radiolysis of water that has resided in the subsurface for a few million years. These concentrations are well above those required to support H_2-utilizing

microorganisms and to inhibit H_2-producing, fermentative microorganisms.

1. Introduction

H_2 is known as one of the most energetic substrates for deep subsurface lithoautotrophic ecosystems (Amend and Shock, 2001; Pedersen, 2000) due to its strong reducing power and diffusivity. H_2-based ecosystems in terrestrial subsurface environments have been proposed (Chapelle et al., 2002; Stevens and Mckinley, 1995). Stevens and McKinley (1995) reported that H_2 produced by the interaction between basalt and groundwater might be sustaining methanogens and acetogens in the Columbia River Basalt aquifer at 1.2 km depth. Chapelle et al. (2002) observed that a microbial ecosystem was dominated by H_2-consuming methanogens at 200 m depth in Lidy Hot Springs, Idaho. The origin of H_2 was proposed to have been generated by active volcanism or seismic activity in deep faults tapping the lower crust (Chapelle et al., 2002). Other H_2 generating mechanisms, such as serpentinization or microbial fermentation, have also been proposed (Coveney et al., 1987; Jackson and Mclnerney, 2002). Regardless of the specific mechanism, long-term subsurface H_2 production through abiotic processes is critical to maintaining an H_2-based subsurface lithoautotrophic ecosystem that is independent from surface photosynthesis.

H_2 constitutes a major component of dissolved inorganic gases (as high as 98% by volume of the total dissolved gases) in the groundwater of Precambrian Shields and its concentration ranges up to several mM (Haveman and Pedersen, 1999; Sherwood Lollar et al., 1993a; Sherwood Lollar et al., 1993b). These concentrations are several orders of magnitude higher than those observed in the studies for marine sediments or shallow

aquifers (Hoehler et al., 1998; Lovely and Goodwin, 1988). Radiolysis of water has been proposed as a mechanism for generating these large quantities of H_2 (Savary and Pagel, 1997; Vovk, 1982). This hypothesis is supported by the observation that H_2-bearing fluid inclusions in quartz are associated with U-bearing minerals (Debussy et al., 1988; Savary and Pagel, 1997).

Energy released from the decay of radioactive elements (e.g. U, Th, and K) dissociates water molecules into H•, OH•, H_2, H_2O_2, a hydrous electron (e_{aq}^-), and H^+ (reaction 1 in Table 1). These products are formed within ~10^{-6} seconds after the primary ionizing event and diffuse into the bulk solution where they react with other aqueous species (see reactions in Table 1). Additional H_2 is formed via the subsequent recombination of 1) two H•, 2) one H• and one e_{aq}^- with one H_2O molecules, and 3) two e_{aq}^- ions with two H_2O molecules (reactions 17, 11 and 10 in Table 1; Spinks and Woods (1990)).

Experimental determinations of the rates of reactions involved in H_2 production (see reviews in Draganic and Draganic (1971) and Spinks and Woods (1990)) have led to theoretical models which extrapolate the H_2 production rate (or yield) over geological time scales. These models suggest that the H_2 yield is constant over a range of dosages (Draganic et al., 1991; Sehested et al., 1973) up to 200 Gray (Gy; 1 Gy = 1 J kg^{-1}) at which point the H_2 yield declines and a maximum H_2 concentration of ~350 nM is attained (Bjergbakke et al., 1989). This steady-state radiolytic H_2 concentration is thought to be derived from the competition between H_2 formation and consumption by OH• (Spinks and Woods, 1990) and occurs well below the solubility limit of H_2 in water under crustal conditions and below the H_2 concentrations observed in the Precambrian

Shield studies mentioned above. According to Bjergbakke et al. (1989), H_2 concentrations greater than this steady state value can only occur if H_2 partitions into an existing gas phase, such as CH_4 or N_2. Bjergbakke et al. (1989) also predicted steady state concentrations for H_2O_2 and O_2 and these have been utilized to predict the impact of radiolytic reactions on microorganisms trapped in single phase, saline fluid inclusions in salt (Kminek et al., 2003).

Previous studies of the isotopic composition of radiolytically produced H• have utilized a combination of scavenging reactions and ^{60}Co γ-irradiated mixtures of H_2O-D_2O (ANBAR and MEYERSTEIN, 1965) and EPR measurements performed on 3 MeV electron pulse-irradiated mixtures of H_2O-D_2O (Bartels et al., 1989). The $\alpha D_{H2O\text{-}H\bullet}$ (the ratio of $(D/H)_{H2O}$ to $(D/H)_{H\bullet}$) ranged from 2 to 3 and was independent of pH up to pH 12 and the ratio of D_2O to H_2O (Anbar and Meyerstein, 1965; Bartels et al., 1989; Hayon, 1965). By using scavengers for OH• (Br^-) and e_{aq}^- (N_2O) to prevent any subsequent reaction between H• and OH•, and H• and e_{aq}^- (reactions 4 and 11 in Table 1), Han and Bartels (1990) were able to attribute the total isotope effect to preferential dissociation of electronically excited HDO* to yield H• with an $\alpha D_{HDO\text{-}H\bullet}$ consistent with that of 2.26 ± 0.10 reported by Anbar and Meyerstein (1966) and recombination of H_3O^+ with e_{aq}^- to yield H• with an $\alpha D_{H2O\text{-}H\bullet} = 3.5 \pm 0.3$ (reactions 15 in Table 1 and 88 in Appendix). Anbar and Meyerstein (1966) have also reported a fractionation value $\alpha D_{H2O\text{-}H2} = 4.7 \pm 0.2$ for the H_2 produced from two e_{aq}^- ions reacting with two H_2O molecules (reactions 10 in Table 1 and 77 and 78 in Appendix), which could potentially mitigate a pH-dependent effect on H_2 isotopic composition. Experimental data on the isotopic fractionation associated with the formation of radiolytic H_2 using mass spectrometry under natural

conditions, i.e. without scavenging reactions, have not been performed to our knowledge.

The purpose of our study was to determine the H_2 yield and the (D/H) value of H_2 under conditions that mimic natural radiolysis in the subsurface. We conducted experiments to characterize the effects of several environmental factors, including accumulated dosage, pH, O_2, and salinity, on the yield and (D/H) of H_2 generated by artificial γ irradiation for pure water. These factors were chosen because the groundwater associated with elevated H_2 occurrences in the Precambrian Shields is highly saline, anaerobic and frequently exhibits elevated pH. These factors also potentially alter the production yields of the H• and OH•. For example, Cl^- reacts with OH• to produce Cl• and OH^- (reaction 39 in Appendix) (Draganic et al., 1991; Sehested et al., 1973) and thereby reduces H_2 consumption by OH• (reaction 9 in Table 1). Both H_2 yield and (D/H) may be significantly altered when compared to radiolysis of pure water. The H_2 yield measured in the laboratory was utilized to calculate the long-term production in the natural settings and to compare the predicted H_2 concentrations to those observed in the field. Finally, the experimentally determined radiolytic fractionation of H_2-H_2O was combined with published isotopic exchange rates for H_2-H_2O to predict the evolution for (D/H) of H_2 produced by natural radiolysis and to compare it to the field observations.

2. Radiolytic experiment

2.1 Sample preparation and irradiation

Samples for artificial γ irradiation included anaerobic water at pH 4, 7, and 10, saline anaerobic water (0.05 M and 0.5 M of NaCl) at pH 7, and aerobic water at pH 7 (Table 2). Stock solutions with different pH were prepared by using 18mΩ water and 0.1

M H_2SO_4 or 0.1 M NaOH for pH adjustment. All of the stock solutions were sterilized before dispensing into serum vials. For the preparation of anaerobic samples, the stock solutions were purged with Ar immediately after autoclaving until room temperature was reached, and subsequently dispensed into serum vials under Ar atmosphere. Aerobic samples were prepared by exposing solutions to air with gentle stirring for one day to saturate with dissolved air. All the vials were sterilized again after being sealed by butyl stoppers. Each sample was prepared in triplicate and consisted of 20 ml of solution and 18 ml of headspace. The samples were irradiated with a ^{60}Co source at a dosage rate of 0.57 Gy sec^{-1} for varying durations. A control sample (an empty vial without H_2O) was irradiated with a dosage of ~1000 Gy to obtain the background H_2 released from the butyl stopper. The (D/H) value of the H_2O before irradiation was 1.4890×10^{-4} (equivalent to δD of –44‰; δD is defined as eq. 1 in Section 2.2).

2.2 Analytical methods

H_2 concentration was measured with a Varian 3300 gas chromatograph (GC) with a 5Å molecular-sieve column and a thermal conductivity detector at the Department of Geology, University of Toronto. Before analyses, samples were shaken vigorously for at least one minute in order to reach an equilibrium state between solution and headspace. Samples were collected by removing 500 μL of headspace gas from serum vials using a gas tight syringe and then injecting it into the GC. The absolute concentration was calibrated to the area of the H_2 peak for the standard gas. The reproducibility was ±5%. The volume concentration of each headspace gas was converted back to the dissolved concentration using Henry's law constant at 25°C (Gordon et al., 1977) and the volume

ratio of solution to headspace.

Hydrogen isotopic composition was measured by injecting 1 ml of headspace gas into a GC-IRMS (isotopic ratio mass spectrometry) system equipped with an HP 6890 GC in line with a Finnigan MAT Delta^{+}-XL IRMS. Hydrogen isotopic composition was expressed as δD value with a reference to the V-SMOW:

$$\delta D‰ = [(D/H)_{sample} / (D/H)_{standard} - 1] \times 1000 \qquad (1)$$

where *D* is deuterium, and the standard is V-SMOW (Craig, 1961). The reproducibility was ±10‰.

2.3 Experimental yield of radiolytic H_2

H_2 concentration exhibited a positive correlation with the applied dosage (Fig. 1a; Table 2). H_2 concentrations for anaerobic samples at pH 7 increased from 46.4 μM to 145.1 μM as the dosages increased from 950 Gy to 3450 Gy. H_2 concentrations for aerobic, low salinity (0.05 M NaCl), high salinity (0.5 M NaCl), low pH (pH 4) and high pH (pH 10) samples with a dosage of ~2000 Gy were 71.4, 79.3, 93.6, 62.0 and 83.1 μM, respectively (Fig. 1a). The control sample did not yield any detectable H_2 (below 1 ppmv of the total gases). The yield derived from the regression of all data points was 0.40 ± 0.04 molecules $(100\ eV)^{-1}$ (solid line in Fig. 1a). The presence of O_2, Cl^-, high H^+ and high OH^- with a dosage of ~2000 Gy varies H_2 yields by 16% (one standard deviation).

2.4 Hydrogen isotopic composition of radiolytic H_2

The δD of H_2 for anaerobic pure water at pH 7 irradiated at different dosages ranged from –510 to –540‰ V-SMOW (Fig. 1b; Table 2). Although the δD of H_2

increases with increasing dosage, the correlation was not considered significant given the analytical uncertainty. For anaerobic water at pH 10, anaerobic saline solutions (0.05 to 0.5 M NaCl) at pH 7, and aerobic water at pH 7, the δD of H_2 ranged from –490 to –540‰ V-SMOW, consistent with those for anaerobic water at pH 7 (Table 2). All of these values are isotopically heavier than the –740‰ V-SMOW predicted for H_2 that has isotopically equilibrated with water at room temperature (Bottinga, 1969). Anaerobic water at pH 4 exhibited δD of –348‰ V-SMOW, significantly heavier than the other measurements.

2.5 Modeling of H_2 yield

The theoretical H_2 yield and isotopic composition were calculated using the H_2O reaction rates of Bjergbakke et al. (1989) modified to include HDO and the Cl^- reaction rates of Draganic et al. (1991) (Table 1 for primary reactions and Appendix for additional isotopic and salinity effects), the primary radical and molecular yields for H_2, H_2O_2, H•, OH•, H^+, and e_{aq}^- from Meesungnoen et al. (2001) (Table 1) and the isotopic fractionations described above (Appendix). We included all the initial conditions (pH, O_2 and Cl^- concentrations and δD of H_2O) used for our experiments. The final yield and isotopic composition of each species was calculated from the summation of the integration of the second-order kinetics from each reaction over a time span using the Kintecus® program.

The modeling revealed a nearly constant H_2 yield as H_2 concentrations increased linearly with respect to the absorbed dosage up to 4000 Gy (dashed line in Fig. 1a). The modeled concentrations were ~1/2 that of the experimental result for anaerobic pure

water at pH 7 and pH 10 (Table 2), but were very similar to the results from aerobic water, anaerobic water with pH 4 and the saline solutions (Table 2).

2.6 Discussion

Bjergbakke et al. (1989) suggested that a steady state H_2 concentration of 350 nM generated by low LET (linear energy transfer) irradiation would be reached when the applied dosage exceeded 200 Gy, because of the kinetic reaction between H_2 and OH• ($H_2 + OH• \rightarrow H_2O + H•$, reaction 9 in Table 1). Our simulations of the same reactions using the same constants, however, failed to reveal any steady state H_2, H_2O_2 or O_2 concentration. We have no explanation for inconsistency between our results and those of Bjergbakke et al. (1989). The fact that our experimental results lie within 50% of our predicted theoretical H_2 concentrations without implementing any correction for H_2 partitioning into the headspace seems to support the reaction constants reported in Bjergbakke et al. (1989) and Draganic et al. (1991).

The δD of H_2 ranged from –490 to –540‰ V-SMOW and yielded no obvious correlation to the applied dosage, pH (except for pH 4), salt content and the presence of O_2. The αD_{H2O-H2} factors ranged from 1.94 to 2.15, which are slightly less than the $\alpha D_{H2O-H•}$ of 2 to 3 measured by Han and Bartel (1990), indicating that H_2 produced in this study was slightly heavier than H•. The modeling yielded a δD of H_2 of –535 ± 20‰ V-SMOW for all simulations (gray area in Fig. 1b). The theoretical uncertainty reflects the uncertainty in the fractionation during the primary yield, 2.26 ± 0.10 (Anbar and Meyerstein, 1966). The uncertainties in the measured fractionation associated with the H_2 produced from two e_{aq}^- reacting with H_2O (reactions 10 in Table 1 and 77 and 78 in

Appendix) and the recombination of H^+ with e_{aq}^- to yield H• (reactions 15 in Table 1 and 88 in Appendix) had no significant impact on the predicted δD of H_2. The difference between our experimental results and previous studies is that the latter focused on D• and H• produced during the first tens of nanoseconds and Br^- was added to scavenge the OH• and inhibit the reaction $H_2 + OH• \rightarrow H_2O + H•$ (reactions 9 in Table 1 and 73 to 76 in Appendix), that consumes radiolytic H_2. This consumption reaction may decompose isotopically lighter H_2 leaving heavier H_2 behind (Anbar and Meyerstein, 1966) and for an $\alpha D_{H2\text{-}H2O}$ of ~2.3 the model yields δD values of H_2 consistent with our experiments. The experiments performed in this study allowed complete reactions between radicals and molecules, diffusion into headspace and presumably yielded the isotopic signature of stable H_2, which more closely mimics the natural subsurface setting.

The reason why the δD (–348‰V-SMOW) for the pH 4 solution was more enriched than the other samples is unclear. Previous experiments indicated that the yields of H• and e_{aq}^- remain constant for water with pH ranging from 2 to 12 (Spinks and Woods, 1990). The probability for the combination of $H• + H• \rightarrow H_2$ (reaction 17 in Table 1), $e_{aq}^- + H• + H_2O \rightarrow OH^- + H_2$ (reaction 11 in Table 1), or $2e_{aq}^- + 2\ H_2O \rightarrow 2\ OH^- + H_2$ (reaction 10 in Table 1) to form H_2 within the reaction spur is constant within this pH range, and hence the isotopic composition would be invariant (Draganic and Draganic, 1971) as confirmed by the modeling results. More experimental work is warranted to determine whether the irradiation of low pH solutions would consistently produce similar results.

3. Modeling of isotopic exchange

To determine whether the heavy δD of radiolytically generated H_2 relative to H_2 that has isotopically equilibrated with water could be used as a diagnostic signature of radiolysis, we modeled the approach to isotopic equilibration given the rates of isotopic exchange and the radiolytic H_2 yield. The kinetic exchange of D between H_2 and H_2O is expressed as a second order reaction:

$$H_2 + HDO \leftrightarrow HD + H_2O \qquad (2)$$

The net production rates of HD and H_2 as a function of time were described in eqs. 3 and 4, respectively:

$$d[HD]/dt = k_f[H_2][HDO] - k_r[HD][H_2O] + G_{HD} \qquad (3)$$

$$d[H_2]/dt = - k_f[H_2][HDO] + k_r[HD][H_2O] + G_{H2} \qquad (4)$$

where k_f and k_r are the forward and backward rate constants at a desired temperature (k_f: 1.18×10^{-10} atm^{-1} sec^{-1} and k_r: 4.26×10^{-10} atm^{-1} sec^{-1} at 20°C), respectively, and G is the radiolytic production of H_2 or HD (the ratio of H_2 to HD production is constant). The backward rate constant was calculated by dividing the equilibrium constant (Bottinga, 1969) with the forward rate constant (Lecluse and Robert, 1994). The forward rate constant and equilibrium constant at a desired temperature can be obtained from eqs. 14 and 15 of Lecluse and Robert (1994), and Table 5 of Bottinga (1969), respectively. The temperature for the calculations was varied from 20 to 90°C, the ambient temperature range for the reported Precambrian Shield gases. Since the δD of radiolytic H_2 was invariant (between –490 to –540‰V-SMOW) among our samples, it was assumed that radiolysis produced H_2 with δD of –500‰V-SMOW in this model. Two scenarios for

isotopic exchange as a function of time were tested: 1) a pulse of –500‰V-SMOW radiolytic H_2 was generated at t = 0 (G_{H2} and G_{HD} = 0) and isotopic exchange between H_2O and produced H_2 followed, and 2) the production of –500‰V-SMOW H_2 and isotopic exchange occurred simultaneously. The δD of H_2O was assumed to be constant (–10‰V-SMOW) due to that the fraction of H_2 produced from H_2O was too small to have a significant impact on total isotopic mass balance of the water for the time duration of the model. The total amount of H_2 (H_2 + HD) for scenario 1 was constant and was linearly increasing with time for scenario 2. The differential equations (eqs. 3 and 4) for the change of HD and H_2 as a function of time were solved separately to derive the analytical solutions. The δD of H_2 at each desired time point was calculated on the basis of the abundances of HD and H_2.

In scenario 1 where H_2 was produced only at the beginning of the exchange experiment and, thereafter, equilibrated with water with δD of –10‰V-SMOW, the δD started to change after the reaction had proceeded for 10^2 years at temperature of 20°C (Fig. 2a). The δD of H_2 was altered quickly to a state of equilibrium with that of water in 10^4 years. Increasing temperature from 20°C to 90°C accelerated the exchange rate and drove the equilibrium isotopic composition of H_2 to heavier values (from –750 to –660‰ V-SMOW). The time required for complete isotopic equilibration dropped significantly to 2×10^2 years at 90°C.

A similar pattern of isotopic exchange was observed for scenario 2 where –500‰ V-SMOW of radiolytic H_2 was continuously produced and exchanged with an infinitely large pool of water with constant δD of –10‰ V-SMOW (Fig. 2b). The temperature posed the same effect by driving δD of H_2 toward the isotopic equilibrium composition.

The time required for isotopic equilibration in scenario 2 was 5×10^5 years for 20°C and 3×10^3 years for 90°C (Fig. 2b). The continuous production of radiolytic H_2 maintained its relatively heavier isotopic composition for a longer period of time. The variation of production rate for H_2 and HD did not change the evolution of δD of H_2 because 1) the production ratio of HD to H_2 was constant, and 2) all the terms in the right side of eqs. 3 and 4 varied in equal proportion. An increase of an order of magnitude in production rate simultaneously increases the rates of both forward and backward exchanges with the same magnitude.

The model for isotopic evolution of radiolytically produced H_2 (Fig. 2) suggests that δD of H_2 can only be used as an indicator of radiolysis for groundwater with residence time less than 10^3 years. For the groundwater with residence time greater than 10^6 years, the δD of H_2 will reach an equilibrium state with that of H_2O, and the paired isotopic compositions should reflect the in-situ temperature. The δD of H_2 (–600 to –710‰ V-SMOW) reported from some Precambrian Shields (Sherwood Lollar et al., 1993b) was heavier than those predicted from the in-situ temperatures and the δD of the groundwater but lighter than those in this experiment, suggesting that the water or H_2 originated at greater depths at higher temperatures. Whether these H_2 is produced by radiolysis or other mechanisms is uncertain due to that the δD of H_2 may be altered significantly given that these highly saline groundwater from Precambrian Shields may potentially possess great residence time on the scale of million years and, therefore, the δD of H_2 would represent the equilibration with that of the groundwater at a specific temperature. The δD of H_2 (–700 to –840‰ V-SMOW) associated with either ophiolites from Oman or sepentinites from Kansas well, however, was consistent with the

equilibrium δD predicted from the δD of groundwater and in-situ temperatures (Coveney et al., 1987; Neal and Stanger, 1983). The close association of these H_2 with ultramafic rocks suggests that the serpentinization is the potential source mechanism for H_2 production at these two sites (Coveney et al., 1987; Neal and Stanger, 1983). Unless the H_2 or groundwater residence time is shorter than 10^3 years and serpentinization produces unique δD of H_2, the observed δD of H_2 would represent the consequence of fast equilibration between H_2 and H_2O, and therefore, dose not allow to draw any direct inference to its origin.

4. Estimation of radiolytic H_2 production of natural settings

To determine whether the H_2 yield determined in this study can produce the high H_2 concentrations observed for the Precambrian Shield environments, the natural dosages for different subsurface environments were derived from the emission of α, β and γ particles released by the decay of U, Th and K. The H_2 yield for γ irradiation obtained in this study (G_{H2}= 0.4 molecules (100 eV)$^{-1}$) was used in the calculations. Slightly higher yields for H_2 were used for α (G_{H2}= 0.96 molecules (100 eV)$^{-1}$) and β (G_{H2}= 0.6 molecules (100 eV)$^{-1}$) irradiations due to their higher energy transfer for exciting water molecules (Harris and Pimblott, 2002). Not all decay energy is available for the production of H_2 due to the interaction between the emitted particles with the minerals (Hoffmann, 1992). The stopping power of minerals was estimated according to eq. 5 (Hoffmann, 1992):

$$E_{net,,i} = E_i \times W \times S_i / (1 + W \times S_i) \qquad (5)$$

where *i* is an α, β, or γ particle, E_{net} is the net dosage absorbed by the pore water (Gy sec^{-}

^{1}) (Table 3), E is the apparent dosage from radiogenic decay (Gy sec^{-1}), W is the weight ratio of pore water to rock (W is 4×10^{-4} when the porosity is 0.1% and the bulk rock density is 2.5 g cm^{-3}), S is the stopping power (S_α = 1.5, S_β = 1.25, S_γ = 1.14) (Hoffmann, 1992). The yield was calculated by eq. 6 (Draganic and Draganic, 1971; Spinks and Woods, 1990):

$$Y = \sum E_{net,,i} \times G_i \qquad (6)$$

where G is H_2 yield per unit of energy and Y is the total yield of H_2. This estimate does not take into account any interfacial energy transfer from the irradiated mineral phase to the water that can lower or enhance H_2 yields, but Petrik et al. (2001) have shown that the presence of SiO_2 had little effect upon the G_{H2}.

Two scenarios were assumed: 1) the porosity is varied as a function of depth as analogous to a hypothesized sedimentary basin and the abundances of radioactive elements are assumed constant along the depth profile; 2) the porosity is assumed constant (0.1%) and the abundances of radioactive elements are varied. In either scenario, the pore space was assumed to be filled with groundwater and interconnected. In scenario 1, the porosity along a depth profile is primarily controlled by the thickness of rock formation above the desired depth according to eq. 7 (Bethke, 1985):

$$\varphi = \varphi_o \, exp \, (-bz) \qquad (7)$$

where φ is the porosity, z is the depth (km), and b is a constant (–0.68 km^{-1}) (Table 3). The depth for calculation was extended from the surface to 5 km and the porosity just below the surface was assumed to be 60%. The concentrations of radioactive elements along a depth profile were assumed constant and were derived from a spontaneous γ log

of a Taylorsville basin borehole (Onstott et al., 1998). In scenario 2, several natural settings with dramatically different concentrations of radioactive elements, including carbon leaders in the Witwatersrand basin (South Africa) (Zumberge et al., 1978), granites in the Fennoscandian Shield (Haapala, 1997), basalts in the Columbia River Basalt province (Lambert et al., 1995), quartzites in the Witwatersrand Supergroup (Nicolaysen et al., 1981), and sediments in the Taylorsville basin (Onstott et al., 1998) were chosen to estimate the radiolytic H_2 production rates (Table 3).

The H_2 yield along a depth profile in a hypothesized sedimentary basin increased from 1.5×10^{-8} nM sec^{-1} to 4.5×10^{-8} nM sec^{-1} as the porosity decreased from 60% to 0.1% (Table 3). Although the decrease in porosity leads to an increase in the bulk concentration of radioactive elements, the apparent bulk dosage does not proportionally increase due to the stopping power of the increasing mineral matrix volume (Hoffmann, 1992). Most of the energetic particles released during radiogenic decay interact with the mineral matrix and are converted to heat. Our calculation suggests that less than 1% of the total energy from radiogenic decay is absorbed directly by the pore water for H_2 generation. H_2 yield is insensitive to porosity.

The radiolytic H_2 production in the five subsurface environments ranged from 10^{-9} to 10^{-4} nM sec^{-1} (Table 3). Since the porosity is assumed constant, only the rock chemistry accounts for the variation in H_2 production rates. The least productive rock unit was the Columbia River basalt, 9.4×10^{-9} nM sec^{-1}, with the H_2 production of the Witwatersrand quartzites of the Witwatersrand Basin being slightly greater at 2.6×10^{-8} nM sec^{-1}.

If groundwater residence time is known, the estimated radiolytic H_2 production

rates can be compared to the measured H_2 concentrations. In the case of groundwater in the Witwatersrand Supergroup encountered in the South African Au mines, the subsurface residence time spans from ~3 to 80 Ma (Lippmann et al., 2003). The radiolytic H_2 production rate of 2.6×10^{-8} nM sec^{-1} equates to a rate of 0.8 mM Ma^{-1}, which for these groundwater ages translates into 2.4 to 64 mM H_2 concentrations. These estimates are within an order of magnitude of measured H_2 concentrations (Lin et al., unpublished data) for the same samples analyzed by Lippmann et al. (2003). This demonstrates that radiolytic H_2 production can account for the observed occurrences of extremely high H_2 concentrations in other Precambrian Shield environments. Other H_2 measurement for deep groundwater in South Africa are orders of magnitude less than the radiolytic prediction (Lin et al., unpublished data). This lack of accumulated radiolytic H_2 suggests the presence of H_2-consuming processes, which is consistent with the microbial origin of CH_4 from these same groundwater samples on the basis of the C and H isotopic compositions of CH_4 (Ward et al., 2004).

5. Implications for microbial metabolisms in the deep biosphere

Our estimates suggest that radiolysis can produce millimolar concentrations of H_2 for every million years of subsurface isolation if there is no consumption. This is at least four orders of magnitude higher than the maximum abundance observed in marine sediments or shallow aquifers (50 nM; Hoehler et al. (1998) and Lovely and Goodwin (1988)). Given the prolonged residence times for groundwater from South African Au mines (Lippmann et al., 2003), a steady state might be reached in which the production rate will be equal to the consumption rate. Potential consumption sources include 1)

microbial H_2-oxidation (with electron acceptors of O_2, Fe^{3+}, SO_4^{2-}, and HCO_3^-) and 2) abiotic processes. H_2-consuming microorganisms benefit from the abundant H_2 due to the increase of available energy, whereas H_2-producing microorganisms, anaerobic fermenters, can be thermodynamically inhibited by the abundant H_2. The free energy available for a specific metabolism is primarily controlled by the quotient derived from the reactant and product concentrations and the free energy in the equilibrium state ($\Delta G_r = \Delta G_r^o + RT \ln Q_r$ where ΔG_r is the free energy for a specific reaction, ΔG_r^o is the free energy in the equilibrium state, R is the gas constant, T is the temperature in Kevin, and Q_r is the reaction quotient) (Hoehler et al., 2002). For H_2-consuming metabolisms, such as sulfate reduction (conversion of SO_4^{2-} to HS^-) and methanogenesis, the stoichiometric ratio of H_2 to electron acceptors (SO_4^{2-} or HCO_3^-) is 4. An increase of H_2 by one order of magnitude would increase the reaction quotient by a power factor four times greater than that for the electron acceptor, assuming that the product concentrations are constant (Hoehler et al., 2002). The free energy available to microorganisms in terrestrial subsurface environments would be driven toward more exergonic conditions (thermodynamic favorable) when compared with those in shallow sedimentary aquifers.

Abiotic formation of hydrocarbons (Sherwood Lollar et al., 2002), lipids (Rushdi and Simoneit, 2001), and organic acids (Cody et al., 2000) have also been proposed by reacting H_2 with CO or CO_2 in the presence of metal sulfide catalysts under hydrothermal conditions. The elevated H_2 abundances from radiolysis also enhance the free energy potentials for these reactions and sustain them over geological time. Potentially these organic compounds can be further utilized by microorganisms to obtain metabolic energy if other electron donors are not available.

Oxidants such as H_2O_2 and O_2 produced during radiolysis have not been detected in the groundwater of the South African Au mines and may be consumed during the cycling of Fe and S. S^{2-} and Fe^{2+} derived from anaerobic microbial metabolisms could be converted abiotically by these oxidants to the oxidized forms. This cycling mechanism would maintain the stability of anaerobic conditions as well as supply the electron acceptors for anaerobic metabolism.

6. Conclusion

Our experimental results indicated that radiolysis produced H_2 in a linearly increasing fashion as the applied dosage increased, which is consistent with our theoretical model. A maximum H_2 concentration was not theoretically as had been reported by previous studies. The δD of radiolytic H_2 ranged from –490 to –540‰ V-SMOW, significantly heavier than that predicted by isotopic equilibration between H_2 and H_2O, and was independent of applied dosage, pH (except for pH 4), dissolved O_2 and Cl^- contents and similar to that predicted theoretically. Calculations of isotopic exchange for D between H_2 and H_2O suggest that δD of H_2 can remain unaltered for less than 10^3 years, but the δD of H_2 reached equilibrium with that of H_2O in less than 10^6 year. The δD of H_2 can only be used as an indicator of radiolysis for groundwater with relatively young age and low temperature. Theoretical calculations also suggest that radiolysis in several natural settings is feasible in producing H_2 at amounts comparable to those reported in the literature from Precambrian crust. Radiolytic H_2 yields predicted by theoretical estimates for several crustal settings are easily sufficient to support lithoautotrophic ecosystems and inhibit fermentative ecosystems in terrestrial subsurface

environments.

Acknowledgments

This work is supported by grant from NSF LExEn program (EAR-9978267) to T.C. Onstott. The authors are grateful to Dr. T. F. Yang of the National Taiwan University for the assistance in measuring the background H_2. We thank Dr. J. P. Amend and three anonymous reviewers for their critical reviews and helpful comments.

References

Amend J. P. and Shock E. L. (2001) Energetics of overall metabolic reactions of thermophilic and hyperthermophilic Archaea and Bacteria. *FEMS Microbiol. Rev.* **25**, 175-243.

Anbar M. and Meyerstein D. (1965) Isotope effect in the radiolysis and photolysis of H_2O-D_2O mixture. *Jour. Phys. Chem.* **69**, 698-700.

Anbar M. and Meyerstein D. (1966) H/D isotope effects in the formation of hydrogen from the combination of two radicals in aqueous solutions. *Trans Fara. Soc.* **62**, 2121-2131.

Bartels D. M., Craw M. T., Han P., and Trifunac A. D. (1989) H/D isotope effects in water radiolysis. 1. Chemically induced dynamic electron polarization in spurs. *Jour. Phys. Chem.* **93**, 2412-2421.

Bethke C. M. (1985) A numerical model of compaction-driven groundwater flow and heat transfer and its application to the paleohydrology of intracratonic sedimentary basins. *Jour. Geophys. Res.* **90**, 6817-6828.

Bjergbakke E., Draganic Z. D., Sehested K., and Draganic I. G. (1989) Radiolytic products in waters. Part I: Computer simulation of some radiolytic processes in the laboratory. *Radiochim. Acta* **48**, 65-71.

Bottinga Y. (1969) Calculated fractionation factors for carbon and hydrogen isotope exchange in the system calcite-CO_2-graphite-methane-hydrogen and water vapour. *Geochim. Cosmochim. Acta* **33**, 49-64.

Chapelle F. H., O'Neill K., Bradley P. M., Methe B. A., Ciufo S. A., Knobel L. L., and Lovely D. R. (2002) A hydrogen-based subsurface microbial community dominated by methanogens. *Nature* **415**, 312-315.

Cody G. D., Boctor N., Blank J., Brandes J., Boctor N., Filley T., Hazen R., and Yoder H. J. (2000) Experimental investigations into dynamic organic reaction networks at high T and P in aqueous media. *Orig. Life Evol. Biosph.* **30**, 187.

Coveney R. M., Jr., Goebel E. D., Zeller E. J., Dreschoff G. A. M., and Angino E. E. (1987) Serpentinization and the origin of hydrogen gas in Kansas. *Amer. Asso. Petrol. Geol.* **71**, 39-48.

Craig H. (1961) Isotopic variations in meteoric waters. *Science* **133**, 1702-1703.

Debussy J., Pagel M., Beny J.-M., Christensen H., Hickel B., Kosztolanyi C., and Poty B. (1988) Radiolysis evidenced by H_2-O_2 and H_2-bearing fluid inclusions in three uranium deposits. *Geochim. Cosmochim. Acta.* **52**, 1155-1167.

Draganic I. G., Bjergbakkw E., Draganic Z. D., and Sehested K. (1991) Decomposition of ocean waters by potassium-40 radiation 3800 Ma ago as a source of oxygen and oxidizing species. *Precambrian Res.* **52**, 337-345.

Draganic I. G. and Draganic Z. D. (1971) *The radiation chemistry of water*. Academic

Press.

Gordon L. I., Cohen Y., and Standley D. R. (1977) The solubility of molecular hydrogen in seawater. *Deep Sea Res.* **24**, 937-941.

Haapala I. (1997) Magmatic and postmagmatic processes in tin-mineralized granites; topaz-bearing leucogranite in the Eurajoki Rapakivi granite stock, Finland. *Jour. Petrol.* **38**, 1645-1659.

Harris R. E. and Pimblott S. M. (2002) On ^{3}H β-particle and ^{60}Co γ irradiation of aqueous systems. *Rad. Res.* **158**, 493-504.

Haveman S. A. and Pedersen K. (1999) Distribution and metabolic diversity of microorganisms in deep igneous rock aquifers of Finland. *Geomicrobiol. Jour.* **16**, 277-294.

Hayon E. (1965) Radiolysis of heavy water in the pD range 0-14. *Jour Phys. Chem.* **69**, 2628-2632.

Hoehler T. M., Alperin M. J., Albert D. B., and Martens C. S. (1998) Thermodynamic control on hydrogen concentrations in anoxic sediments. *Geochim. Cosmochim. Acta* **62**(10), 1745-1756.

Hoehler T. M., Bebout B. M., and Marais D. J. D. (2002) The role of microbial mats in the production of reduced gases on the early Earth. *Nature* **412**, 324-327.

Hoffmann B. A. (1992) Isolated reduction phenomenon in red beds: A result of porewater radiolysis. In *Water-rock interaction* (ed. Y. K. Kharaka and A. S. Maest), pp. 503-506. Rotterdam/Brookfield.

Jackson B. E. and Mclnerney M. J. (2002) Anaerobic microbial metabolism can proceed close to thermodynamic limits. *Nature* **415**, 454-456.

Kminek G., Bada J., Polgliano K., and Ward J. F. (2003) Radiation dependent limit for the viability of bacterial spores in halite fluid inclusions and on Mars. *Rad. Res.* **159**, 722-729.

Lambert R., Chamberlain V. E., and Holland J. G. (1995) Ferro-andesites in the Grande Ronde Basalt; their composition and significance in studies of the origin of the Columbia River Basalt Group. *Can. Jour. Earth Sci.* **32**, 424-436.

Lecluse C. and Robert F. (1994) Hydrogen isotope exchange reaction rates: Origin of water in the inner solar system. *Geochim. Cosmochim. Acta* **58**, 2927-2939.

Lippmann J., Stute M., Torgersen T., Moser D. P., Hall J., Lin L.-H., Borcsik M., Bellamy R. E. S., and Onstott T. C. (2003) Dating ultra-deep mine waters with noble gases and ^{36}Cl, Witwatersrand Basin, South Africa. *Geochim. Cosmochim. Acta* **67**, 4597-4619.

Lovely D. R. and Goodwin S. (1988) Hydrogen concentrations as an indicator of the predominant terminal electron-accepting reaction in aquatic sediments. *Geochim. Cosmochim. Acta* **52**, 2993-3003.

Meesungnoen J., Benrahmoune M., Filali-Mouhim A., Mankhetkorn S., and Jay-gerin J.-P. (2001) Monte Carlo calculation of the primary radical and molecular yields of liquid water radiolysis in the linear energy transfer range 0.3 - 6.5 keV/mm: Application to ^{137}Cs gamma rays. *Rad. Res.* **155**, 269-278.

Neal C. and Stanger G. (1983) Hydrogen generation from mantle source rocks in Oman. *Earth Planet. Sci. Lett.* **60**, 315-321.

Nicolaysen L. O., Hart R. J., and Gale N. H. (1981) The Vredefort radioelement profile extended to supracrustal strata at Carletonville, with implications for continental

heat flow. *Jour. Geophys. Res.* **86**, 10653-10661.

Onstott T. C., Phelps T. J., Colwell F. S., Ringeberg D., White D. C., and Boone D. R. (1998) Observations pertaining to the origin and ecology of microorganisms recovered from the deep subsurface of Taylorsville basin, Virginia. *Geomicrobiol. Jour.* **15**, 353-385.

Pedersen K. (2000) Exploration of deep intraterrestrial microbial life: current perspectrives. *FEMS Microbiol. Lett.* **185**, 9-16.

Petrik N. G., Alexandrov A. B., and Vall A. I. (2001) Interfacial energy transfer during gamma radiolysis of water on the surface of ZrO_2 and some other oxides. *Jour. Phys. Chem. B* **105**, 5935-5944.

Rushdi A. I. and Simoneit B. R. T. (2001) Lipid formation by aqueous Fischer-Tropsch-type synthesis over a temperature range of 100 to 400 ^{o}C. *Orig. Life Evol. Biosph.* **31**, 103-118.

Savary V. and Pagel M. (1997) The effects of water radiolysis on local redox conditions in the Oklo, Gabon, natural fission reactors 10 and 16. *Geochim. Cosmochim. Acta* **61**, 4479-4494.

Sehested K., Bjergbakke E., and Fricke H. (1973) The primary species yields in the ^{60}Co γ-ray radiolysis of aqueous solutions of H_2SO_4 between pH 7 and 0.46. *Rad. Res.* **56**, 385-399.

Sherwood Lollar B., Frape S. K., Fritz P., Macko A., Welhan J. A., Blomovist R., and Lahermo P. W. (1993a) Evidence for bacterially generated hydrocarbon gas in Canadian shield and Fennoscandian shield rocks. *Geochim. Cosmochim. Acta* **57**, 5071-5085.

Sherwood Lollar B., Frape S. K., Weise S. M., Fritz P., Macko A., and Weilhan J. A. (1993b) Abiogenic methanogenesis in crystalline rocks. *Geochim. Cosmochim. Acta* **57**, 5087-5097.

Sherwood Lollar B., Westgate T. D., Ward J. A., Slater G. F., and Lacrampe-Couloume G. (2002) Abiogenic formation of alkanes in the Earth's crust as a minor source for global hydrocarbon reservoirs. *Nature* **416**, 522-524.

Spinks J. W. T. and Woods R. J. (1990) *An introduction to radiation chemistry*. John Wiley & Sons.

Stevens T. O. and McKinley J. P. (1995) Lithoautotrophic microbial ecosystems in deep basalt aquifers. *Science* **270**, 450-454.

Vovk I. F. (1982) Radiolysis of underground waters as the mechanism of geochemical transformation of the energy of radioactive decay in sedimentary rocks. *Litho. Mineral. Res.*, 328-334.

Ward J. A., Slater G. F., Moser D., Lin L.-H., Lacrampe-Couloume G., Bonin A., Davidson, M., Hall J., Mislowack, B., Onstott T. C., and Sherwood Lollar B. (2004) Microbial hydrocarbon gases in the Witwatersrand Basin, South Africa: Implications for the deep biosphere. *Geochim. Cosmochim. Acta* (in press).

Zumberge J. E., Sigleo A. C., and Nagy B. (1978) Molecular and elemental analyses of the carbonaceous matter in the gold- and uranium-bearing Vaal Reef carbon seams, Witwatersrand Sequence. *Mineral. Sci. Engineer.* **10**, 233-246.

Table 1 Primary radiolytic reactions and rate constants for theoretical modeling[1]

No.	Reaction	Rate constant (M^{-1} sec^{-1})
1	$4.16\ H_2O \rightarrow 2.66\ e_{aq}^- + 2.66\ H^+ + 0.45\ H_2 + 0.60\ H\bullet + 0.68\ H_2O_2 + 2.80\ OH\bullet$	5.90E-08
2	$2\ OH\bullet \rightarrow H_2O_2$	6.00E+09
3	$OH\bullet + e_{aq}^- \rightarrow OH^-$	2.50E+10
4	$OH\bullet + H\bullet \rightarrow H_2O$	2.50E+10
5	$OH\bullet + HO_2\bullet \rightarrow O_2 + H_2O$	7.90E+09
6	$OH\bullet + O_2^- \rightarrow OH^- + O_2$	1.00E+10
7	$OH\bullet + H_2O_2 \rightarrow H_2O + O_2^- + H^+$	2.70E+07
8	$OH\bullet + HO_2^- \rightarrow H_2O + O_2^-$	7.50E+09
9	$OH\bullet + H_2 \rightarrow H_2O + H\bullet$	4.00E+07
10	$2\ e_{aq}^- + 2\ H_2O \rightarrow 2\ OH^- + H_2$	6.00E+09
11	$e_{aq}^- + H\bullet + H_2O \rightarrow OH^- + H_2$	2.00E+10
12	$e_{aq}^- + O_2^- + H_2O \rightarrow HO_2^- + OH^-$	1.20E+10
13	$e_{aq}^- + HO_2^- \rightarrow O^- + OH^-$	3.50E+09
14	$e_{aq}^- + H_2O_2 \rightarrow OH\bullet + OH^-$	1.60E+10
15	$e_{aq}^- + H^+ \rightarrow H\bullet$	2.20E+10
16	$e_{aq}^- + O_2 \rightarrow O_2^-$	2.00E+10
17	$2\ H\bullet \rightarrow H_2$	1.00E+10
18	$H\bullet + HO_2\bullet \rightarrow H_2O_2$	2.00E+10
19	$H\bullet + O_2^- \rightarrow HO_2^-$	2.00E+10
20	$H\bullet + H_2O_2 \rightarrow OH\bullet + H_2O$	6.00E+07
21	$H\bullet + OH^- \rightarrow H_2O + e^-$	1.50E+07
22	$H\bullet + O_2 \rightarrow O_2^- + H^+$	2.00E+10
23	$H\bullet + O^- \rightarrow OH^-$	2.00E+10
24	$2\ O^- + 2\ H_2O \rightarrow H_2O_2 + 2\ OH^-$	9.00E+08
25	$O^- + O_2^- + H_2O \rightarrow O_2 + 2\ OH^-$	6.00E+08
26	$O^- + O_3^- \rightarrow 2\ O_2^-$	7.00E+08
27	$O^- + H_2O_2 \rightarrow O_2^- + H_2O$	5.00E+08
28	$O^- + HO_2^- \rightarrow O_2^- + OH^-$	5.00E+08
29	$O^- + H_2O \rightarrow OH\bullet + OH^-$	2.00E+06
30	$O^- + O_2 \rightarrow O_3^-$	3.00E+09
31	$O^- + H_2 \rightarrow H\bullet + OH^-$	2.00E+08
32	$2\ HO_2\bullet \rightarrow O_2 + H_2O_2$	7.50E+05
33	$HO_2\bullet + O_2^- \rightarrow O_2 + HO_2^-$	1.00E+08
34	$O_3^- \rightarrow O^- + O_2$	3.30E+03
35	$O_3^- + H^+ \rightarrow OH\bullet + O_2$	9.00E+10
36	$H_2O \rightarrow H^+ + OH^-$	2.60E-05[2]
37	$H^+ + OH^- \rightarrow H_2O$	1.44E+11

[1]Reactions 2 to 35 are from Bjergbakke et al. (1989).

[2]Reactions 36 and 37 define the K_a of the reaction $H_2O \rightarrow H^+ + OH^-$.

Table 2 Sample characteristics, H_2 yields and δD of H_2

Sample No.	pH	Solute and headspace	Dosages (Gy)	Measured H_2 Yield (μM)[1]	Predicted H_2 Yield (μM)[2]	δD of H_2-$_{V\text{-}SMOW}$ (‰)[3]
1	7	anaerobic	952	46.4 ± 1.9	18.6 ± 0.3	-536 ± 1
2	7	anaerobic	1808	78.7 ± 1.2	31.8 ± 0.6	-524 ± 10
3	7	anaerobic	2820	108.2 ± 4.7	49.4 ± 0.9	-510 ± 7
4	7	anaerobic	3450	145.1 ± 6.7	60.2 ± 1.0	-511 ± 3
5	4	anaerobic	1890	62.0 ± 1.9	65.4 ± 0.6	-348 ± 8
6	10	anaerobic	1890	83.1 ± 3.8	34.7 ± 0.6	-511 ± 6
7	7	anaerobic 0.05M NaCl	2072	79.3 ± 2.6	95.2 ± 0.7	N/A
8	7	Anaerobic 0.5 M NaCl	2072	93.6 ± 0.9	95.1 ± 0.7	-539 ± 6
9	7	aerobic	1900	71.4 ± 0.9	84.3 ± 0.6	-490 ± 3

[1] The uncertainties were based on one standard deviation for triplicate analyses.

[2] The uncertainties were based on one standard deviation in the yield coefficients (per 100 eV) for 4.16 $H_2O \rightarrow 2.66\ e_{aq}^- + 2.66\ H^+ + 0.45\ H_2 + 0.60\ H\bullet + 0.68\ H_2O_2 + 2.80\ OH\bullet$.

[3] The δD of H_2O before irradiation was –44‰.

Table 3 Calculations for the net dosage rates and radiolytic H_2 yield rates in natural settings

Rock type location	Porosity (%)	U (ppm)	Th (ppm)	K (%)	α dose rate (Gy sec^{-1})	β dose rate (Gy sec^{-1})	γ dose rate (Gy sec^{-1})	H_2 rate (nM sec^{-1})	Data source
Carbon leaders South Africa	0.1	40000	8000	1	4.3×10^{-6}	2.4×10^{-11}	5.0×10^{-8}	2.0×10^{-4}	Zumberge et al., 1978
Granites Fennoscandian Shield	0.1	10	30	5.0	1.7×10^{-9}	1.2×10^{-10}	6.8×10^{-11}	9.0×10^{-8}	Haapala, 1997
Basalts Columbia River Basalt	0.1	1	3	0.8	1.7×10^{-10}	1.9×10^{-11}	9.7×10^{-12}	9.4×10^{-9}	Lambert et al., 1995
Quartzites Witwatersrand Supergroup	0.1	2	11	2	4.9×10^{-11}	4.6×10^{-11}	2.4×10^{-11}	2.6×10^{-8}	Nicolaysen et al., 1981
Sediments Taylorsville Basin[1]	0.1	5	15	2.5	8.7×10^{-10}	6.5×10^{-11}	3.4×10^{-11}	4.5×10^{-8}	Onstott et al., 1998
	60				5.4×10^{-10}	3.8×10^{-11}	2.1×10^{-11}	1.5×10^{-8}	

Figure captions

Figure 1 Plot of radiolytic H_2 yield (a) and δD of H_2 (b) versus the applied dosage (Gy). Solid line and dashed line in (a) showed the yield of 0.4 molecules $(100\ eV)^{-1}$ and theoretical prediction for anaerobic solution at pH 7, respectively. Gray area in (b) showed the theoretical prediction.

Figure 2 Plot of deuterium exchange between H_2 and H_2O as a function of time for different temperatures (20 to 90^{o}C). The δD of H_2O was assumed constant (-10‰ V-SMOW). (a) A pulse production of H_2 with δD of –500‰ V-SMOW at t = 0. (b) Continuous production of H_2 with δD of –500‰ V-SMOW at a rate of 1 nM yr^{-1}.

Appendix Complete radiolytic reactions and rate constants for theoretical modeling[1]

No.	Reaction	Rate constant (M^{-1} sec^{-1})
1	4.16 $H_2O \rightarrow$ 2.66 e_{aq}^- + 2.66 H^+ + 0.45 H_2 + 0.60 H• +0.68 H_2O_2 + 2.80 OH•	5.90E-08
2	4.16 HDO $\rightarrow$ 2.66 e_{aq}^- + 2.66 (H^+) D^+ + 0.45 HD + 0.60 (H•) D• +0.68 HDO_2 + 2.80 (OH•) OD•	1.87E-13/2.26[2]
3	2 OH• $\rightarrow$ H_2O_2	6.00E+09
4	OH• + e_{aq}^- $\rightarrow$ OH^-	2.50E+10
5	OH• + H• $\rightarrow$ H_2O	2.50E+10
6	OH• + HO_2• $\rightarrow$ O_2 + H_2O	7.90E+09
7	OH• + O_2^- $\rightarrow$ OH^- + O_2	1.00E+10
8	OH• + H_2O_2 $\rightarrow$ H_2O + O_2^- + H^+	2.70E+07
9	OH• + HO_2^- $\rightarrow$ H_2O + O_2^-	7.50E+09
10	OH• + H_2 $\rightarrow$ H_2O + H•	4.00E+07
11	2 e_{aq}^- + 2 H_2O $\rightarrow$ 2 OH^- + H_2	6.00E+09
12	e_{aq}^- + H• + H_2O $\rightarrow$ OH^- + H_2	2.00E+10
13	e_{aq}^- + O_2^- + H_2O $\rightarrow$ HO_2^- + OH^-	1.20E+10
14	e_{aq}^- + HO_2^- $\rightarrow$ O^- + OH^-	3.50E+09
15	e_{aq}^- + H_2O_2 $\rightarrow$ OH• + OH^-	1.60E+10
16	e_{aq}^- + H^+ $\rightarrow$ H•	2.20E+10
17	e_{aq}^- + O_2 $\rightarrow$ O_2^-	2.00E+10
18	2 H• $\rightarrow$ H_2	1.00E+10
19	H• + HO_2• $\rightarrow$ H_2O_2	2.00E+10
20	H• + O_2^- $\rightarrow$ HO_2^-	2.00E+10
21	H• + H_2O_2 $\rightarrow$ OH• + H_2O	6.00E+07
22	H• + OH^- $\rightarrow$ H_2O + e^-	1.50E+07
23	H• + O_2 $\rightarrow$ O_2^- + H^+	2.00E+10
24	H• + O^- $\rightarrow$ OH^-	2.00E+10
25	2 O^- + 2 H_2O $\rightarrow$ H_2O_2 + 2 OH^-	9.00E+08
26	O^- + O_2^- + H_2O $\rightarrow$ O_2 + 2 OH^-	6.00E+08
27	O^- + O_3^- $\rightarrow$ 2 O_2^-	7.00E+08
28	O^- + H_2O_2 $\rightarrow$ O_2^- + H_2O	5.00E+08
29	O^- + HO_2^- $\rightarrow$ O_2^- + OH^-	5.00E+08
30	O^- + H_2O $\rightarrow$ OH• + OH^-	2.00E+06
31	O^- + O_2 $\rightarrow$ O_3^-	3.00E+09
32	O^- + H_2 $\rightarrow$ H• + OH^-	2.00E+08
33	2 HO_2• $\rightarrow$ O_2 + H_2O_2	7.50E+05
34	HO_2• + O_2^- $\rightarrow$ O_2 + HO_2^-	1.00E+08
35	O_3^- $\rightarrow$ O^- + O_2	3.30E+03
36	O_3^- + H^+ $\rightarrow$ OH• + O_2	9.00E+10
37	H_2O $\rightarrow$ H^+ + OH^-	2.60E-05[3]
38	H^+ + OH^- $\rightarrow$ H_2O	1.44E+11

39	$OH\bullet + Cl^- \rightarrow Cl\bullet + OH^-$	4.30E+09
40	$e_{aq}^- + Cl\bullet \rightarrow Cl^-$	1.00E+10
41	$e_{aq}^- + Cl_2^- \rightarrow 2\ Cl^-$	1.00E+10
42	$e_{aq}^- + ClOH^- \rightarrow Cl^- + OH^-$	1.00E+10
43	$e_{aq}^- + Cl_2 \rightarrow Cl_2^-$	1.00E+10
44	$H\bullet + Cl\bullet \rightarrow Cl^- + H^+$	1.00E+10
45	$H\bullet + Cl_2^- \rightarrow 2\ Cl^- + H^+$	8.00E+09
46	$H\bullet + ClOH^- \rightarrow Cl^- + H_2O$	1.00E+10
47	$H\bullet + Cl_2 \rightarrow Cl_2^- + H^+$	7.00E+09
48	$HO_2 + Cl_2^- \rightarrow 2\ Cl^- + O_2 + H^+$	4.00E+09
49	$HO_2 + Cl_2 \rightarrow Cl_2^- + O_2 + H^+$	1.00E+09
50	$O_2^- + Cl_2^- \rightarrow 2\ Cl^- + O_2$	1.20E+10
51	$H_2O_2 + Cl_2^- \rightarrow 2\ Cl^- + O_2^- + 2\ H^+$	1.40E+05
52	$H_2O_2 + Cl_2 \rightarrow HO2 + Cl_2^- + H^+$	1.90E+02
53	$OH^- + Cl_2^- \rightarrow ClOH^- + Cl^-$	7.30E+06
54	$H^+ + ClOH^- \rightarrow Cl\bullet + H_2O$	2.10E+10
55	$Cl^- + Cl\bullet \rightarrow Cl_2^-$	2.10E+10
56	$Cl^- + ClOH^- \rightarrow Cl_2^- + OH^-$	9.00E+04
57	$ClOH^- \rightarrow OH\bullet + Cl^-$	6.10E+09
58	$Cl_2^- \rightarrow Cl\bullet + Cl^-$	1.10E+05
59	$2\ Cl_2^- \rightarrow Cl_2 + 2\ Cl^-$	7.00E+09
60	$OD + OH\bullet \rightarrow HDO_2$	6.00E+09
61	$OD\bullet + e_{aq}^- \rightarrow OD^-$	2.50E+10
62	$OD\bullet + H\bullet \rightarrow HDO$	2.50E+10
63	$OH\bullet + D\bullet \rightarrow HDO$	2.50E+10
64	$OD\bullet + HO_2\bullet \rightarrow O_2 + HDO$	7.90E+09
65	$OH\bullet + DO_2\bullet \rightarrow O_2 + HDO$	7.90E+09
66	$OD\bullet + O_2^- \rightarrow OD^- + O_2$	1.00E+10
67	$OH\bullet + HDO_2 \rightarrow HDO + O_2^- + H^+$	2.70E+07
68	$OH\bullet + HDO_2 \rightarrow H_2O + O_2^- + D^+$	2.70E+07
69	$OD\bullet + H_2O_2 \rightarrow HDO + O_2^- + H^+$	2.70E+07
70	$OD\bullet + H_2O_2 \rightarrow H_2O + O_2^- + D^+$	2.70E+07
71	$OH\bullet + DO_2^- \rightarrow HDO + O_2^-$	7.50E+09
72	$OD\bullet + HO_2^- \rightarrow HDO + O_2^-$	7.50E+09
73	$OD\bullet + H_2 \rightarrow HDO + H\bullet$	4.00E+07/2.3
74	$OD\bullet + H_2 \rightarrow H_2O + D\bullet$	4.00E+07/2.3
75	$OH\bullet + HD \rightarrow HDO + H\bullet$	4.00E+07/2.3
76	$OH\bullet + HD \rightarrow H_2O + D\bullet$	4.00E+07
77	$2\ e_{aq}^- + H_2O + HDO \rightarrow 2\ OH^- + HD$	6.00E+09/4.7
78	$2\ e_{aq}^- + H_2O + HDO \rightarrow OH^- + OD^- + H_2$	6.00E+09
79	$e_{aq}^- + D\bullet + H_2O \rightarrow OD^- + H_2$	2.00E+10
80	$e_{aq}^- + D\bullet + H_2O \rightarrow OH^- + HD$	2.00E+10
81	$e_{aq}^- + H\bullet + HDO \rightarrow OD^- + H_2$	2.00E+10
82	$e_{aq}^- + H\bullet + HDO \rightarrow OH^- + HD$	2.00E+10

83	$e_{aq}^- + O_2^- + HDO \rightarrow DO_2^- + OH^-$	1.20E+10
84	$e_{aq}^- + O_2^- + HDO \rightarrow HO_2^- + OD^-$	1.20E+10
85	$e_{aq}^- + DO_2^- \rightarrow O^- + OD^-$	3.50E+09
86	$e_{aq}^- + HDO_2 \rightarrow OD\bullet + OH^-$	1.60E+10
87	$e_{aq}^- + HDO_2 \rightarrow OH\bullet + OD^-$	1.60E+10
88	$e_{aq}^- + D^+ \rightarrow D\bullet$	2.20E+10/3.5
89	$H\bullet + D\bullet \rightarrow HD$	1.00E+10
90	$H\bullet + DO_2\bullet \rightarrow HDO_2$	2.00E+10
91	$D\bullet + HO_2\bullet \rightarrow HDO_2$	2.00E+10
92	$D\bullet + O_2^- \rightarrow DO_2^-$	2.00E+10
93	$H\bullet + HDO_2 \rightarrow OD\bullet + H_2O$	6.00E+07
94	$H\bullet + HDO_2 \rightarrow OH\bullet + HDO$	6.00E+07
95	$D\bullet + H_2O_2 \rightarrow OD\bullet + H_2O$	6.00E+07
96	$D\bullet + H_2O_2 \rightarrow OH\bullet + HDO$	6.00E+07
97	$H\bullet + OD^- \rightarrow HDO + e^-$	1.50E+07
98	$D\bullet + OH^- \rightarrow HDO + e^-$	1.50E+07
99	$D\bullet + O_2 \rightarrow O_2^- + D^+$	2.00E+10
100	$D\bullet + O^- \rightarrow OD^-$	2.00E+10
101	$2\ O^- + H_2O + HDO \rightarrow HDO_2 + 2\ OH^-$	9.00E+08
102	$2\ O^- + H_2O + HDO \rightarrow H_2O_2 + OH^- + OD^-$	9.00E+08
103	$O^- + O_2^- + HDO \rightarrow O_2 + OH^- + OD^-$	6.00E+08
104	$O^- + HDO_2 \rightarrow O_2^- + HDO$	5.00E+08
105	$O^- + DO_2^- \rightarrow O_2^- + OD^-$	5.00E+08
106	$O^- + HDO \rightarrow OD\bullet + OH^-$	2.00E+06
107	$O^- + HDO \rightarrow OH\bullet + OD^-$	2.00E+06
108	$O^- + HD \rightarrow H\bullet + OD^-$	2.00E+08
109	$O^- + HD \rightarrow D\bullet + OH^-$	2.00E+08
110	$HO_2\bullet + DO_2\bullet \rightarrow O_2 + HDO_2$	7.50E+05
111	$DO_2\bullet + O_2^- \rightarrow O_2 + DO_2^-$	1.00E+08
112	$O_3^- + D^+ \rightarrow OD\bullet + O_2$	9.00E+10
113	$OD\bullet + Cl^- \rightarrow Cl\bullet + OD^-$	4.30E+09
114	$e_{aq}^- + ClOD^- \rightarrow Cl^- + OD^-$	1.00E+10
115	$D\bullet + Cl\bullet \rightarrow Cl^- + D^+$	1.00E+10
116	$D\bullet + Cl_2^- \rightarrow 2\ Cl^- + D^+$	8.00E+09
117	$H\bullet + ClOD^- \rightarrow Cl^- + HDO$	1.00E+10
118	$D\bullet + ClOH^- \rightarrow Cl^- + HDO$	1.00E+10
119	$D\bullet + Cl_2 \rightarrow Cl_2^- + D^+$	7.00E+09
120	$DO_2 + Cl_2^- \rightarrow 2\ Cl^- + O_2 + D^+$	4.00E+09
121	$DO_2 + Cl_2 \rightarrow Cl_2^- + O_2 + D^+$	1.00E+09
122	$HDO_2 + Cl_2^- \rightarrow 2\ Cl^- + O_2^- + H^+ + D^+$	1.40E+05
123	$HDO_2 + Cl_2 \rightarrow DO2 + Cl_2^- + H^+$	1.90E+02
124	$HDO_2 + Cl_2 \rightarrow HO2 + Cl_2^- + D^+$	1.90E+02
125	$OD^- + Cl_2^- \rightarrow ClOD^- + Cl^-$	7.30E+06
126	$D^+ + ClOH^- \rightarrow Cl\bullet + HDO$	2.10E+10

127	$H^+ + ClOD^- \rightarrow Cl\bullet + HDO$	2.10E+10
128	$Cl^- + ClOD^- \rightarrow Cl_2^- + OD^-$	9.00E+04
129	$ClOD^- \rightarrow OD\bullet + Cl^-$	6.10E+09

[1]Reactions 3 to 36 are from Bjergbakke et al. (1989) and reactions 37 to 59 from Draganic et al. (1991).

[2]Primary radiolytic rate based upon same dosage rate as reaction 1 multiplied by the concentration of HDO derived for the isotopic composition of the water ($\delta D = -44^o/_{oo}$ V-SMOW).

[3]Reactions 37 and 38 define the K_a of the reaction $H_2O \rightarrow H^+ + OH^-$.

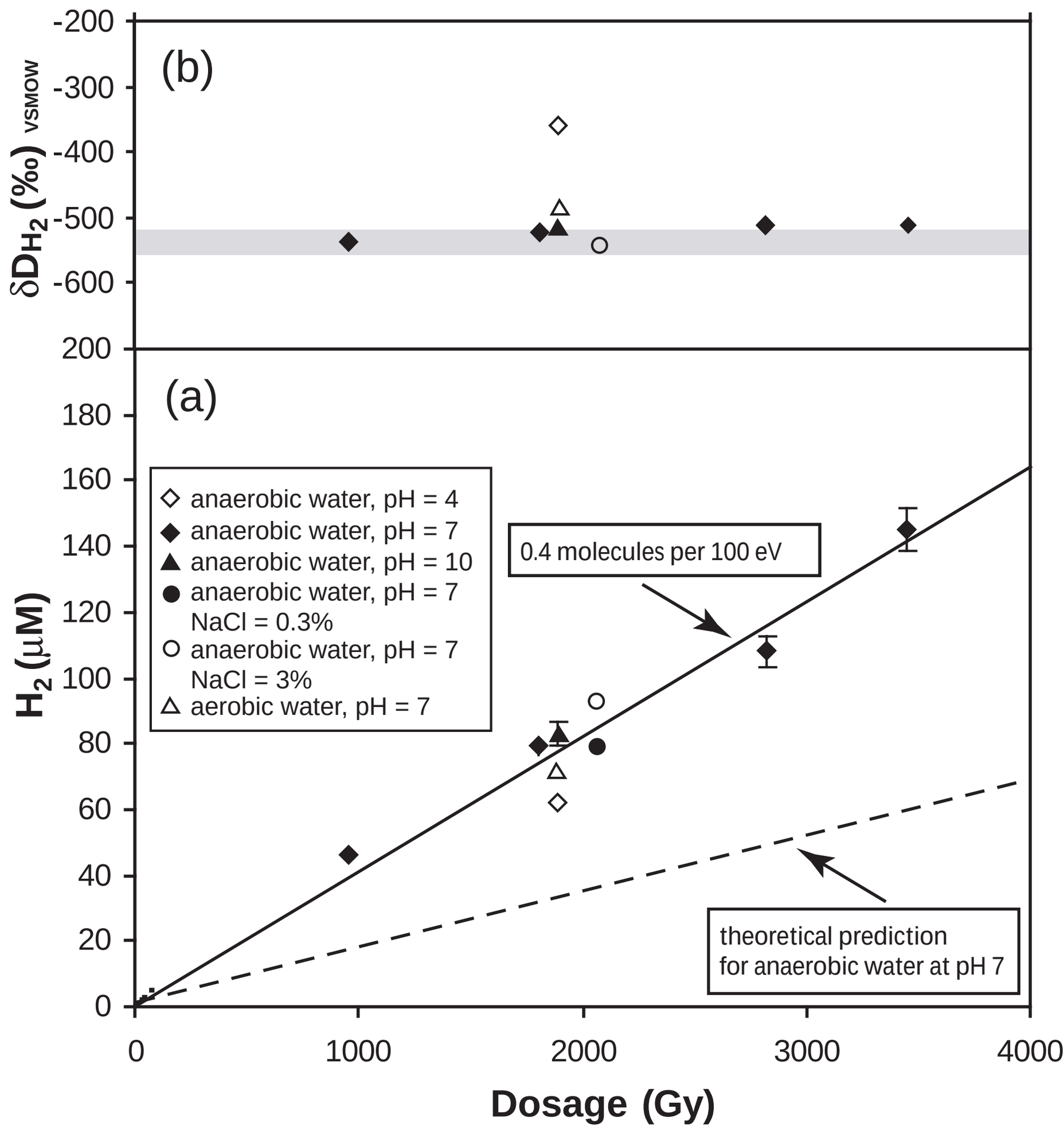
(b)
(a)
δD_{H_2} (‰) VSMOW
H_2 (μM)
Dosage (Gy)
anaerobic water, pH = 4
anaerobic water, pH = 7
anaerobic water, pH = 10
anaerobic water, pH = 7 NaCl = 0.3%
anaerobic water, pH = 7 NaCl = 3%
aerobic water, pH = 7
0.4 molecules per 100 eV
theoretical prediction for anaerobic water at pH 7

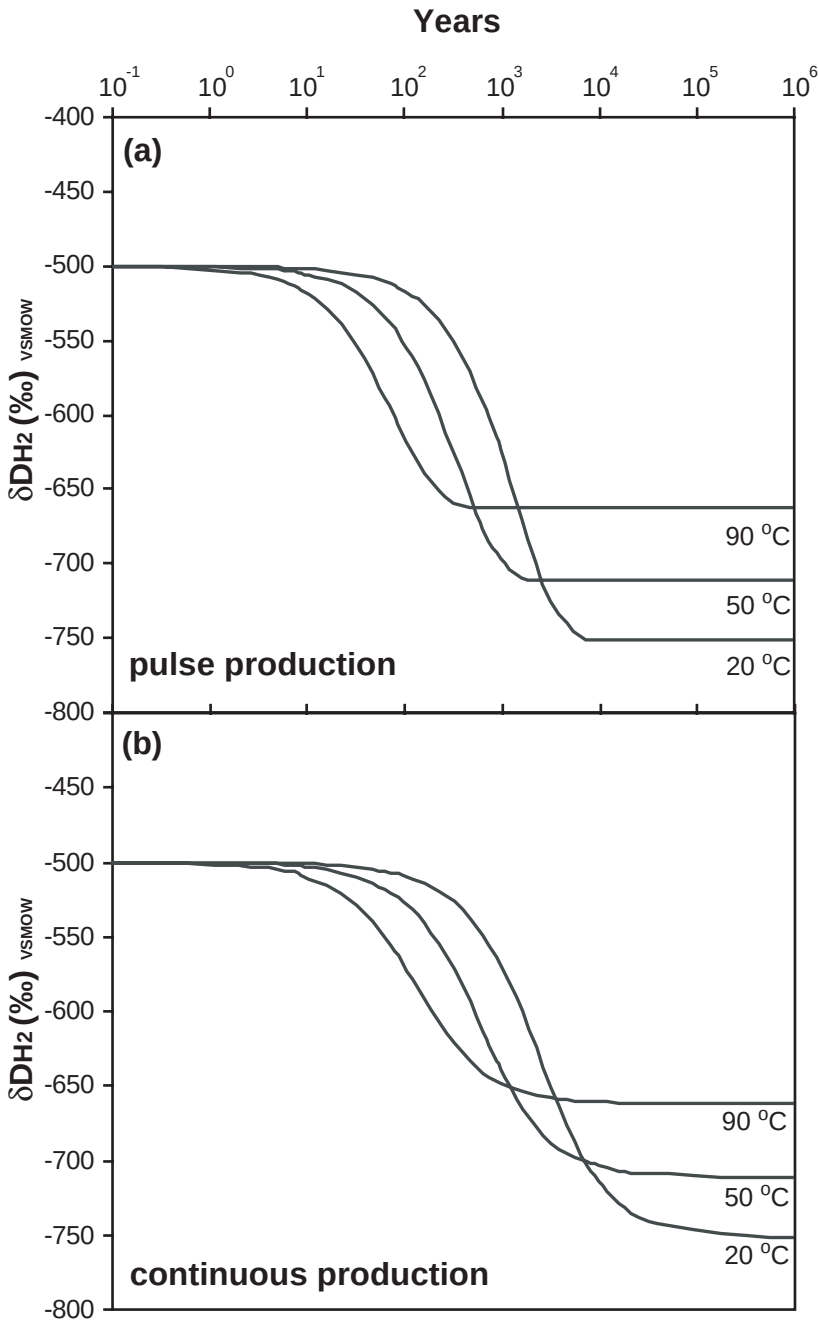
Years
10-1
100
101
102
103
104
105
106
(a)
-400
-450
-500
-550
-600
-650
-700
-750
-800
δDH2 (‰) VSMOW
90 °C
50 °C
20 °C
pulse production
(b)
-450
-500
-550
-600
-650
-700
-750
-800
δDH2 (‰) VSMOW
90 °C
50 °C
20 °C
continuous production